

395820

Large-eddy simulation of flow through a plane, asymmetric diffuser

By Hans-Jakob Kaltenbach

1. Motivation and objectives

A challenge for traditional turbulence modeling, based on the Reynolds averaged Navier-Stokes equations, remains the accurate prediction of 'mild', adverse pressure-gradient driven separation from a smooth surface. Durbin (1994) showed recently that his modified $k - \epsilon$ -model, which carries the wall-normal Reynolds stress as additional velocity scale, is superior to a variety of more complicated Reynolds stress models in its capability to predict 'mild' separation.

With this study we want to explore the capability of large-eddy simulation to predict the separation which occurs on the deflected wall of an asymmetric, plane diffuser with opening angle of 10° . Simpson (1989) points out that 'mild' separation of a boundary layer under the influence of an external pressure gradient leads to a growth of turbulent length scales and generally increases the turbulence level. He emphasizes the role of 'coherent' motion elements for the process of separation. Smoke visualization has revealed that the zone of mean backflow strongly interacts with the forward flow in the above layer. In the mean backflow region, the flow reverses sign quite often, indicating strong intermittency. These features are difficult to capture with statistical models which are based on mean velocity gradients such as mixing length approaches. Conversely, one can expect that LES which explicitly resolves the large motion elements should be able to correctly represent this aspect of separated flows.

The flow through the plane diffuser - which is depicted in Fig. 1- exhibits some additional interesting physical phenomena which make it a challenging test case. In addition to 'mild' separation about halfway down the deflected ramp, the flow is characterized by a small backflow zone with stalled fluid in the rear part of the expanding section. The turbulent flow entering the diffuser is subject to combined adverse and radial pressure gradients stemming from the convex curvature. Finally the flow recovers into a developed, turbulent channel flow in the outlet section.

Obi *et al.* (1993) provide measurements of mean flow, Reynolds stresses, and pressure recovery, which were obtained by means of LDV in a wind tunnel. The details of the experiment and the suitability of the measurements for validation purposes will be discussed in section 2.4.

The objective of this study is to investigate whether LES with the standard dynamic model is able to accurately predict the flow in the one-sided diffuser and to explore the resolution requirements and associated costs.

PRECEDING PAGE BLANK NOT FILMED

PAGE 174 INTENTIONALLY BLANK



FIGURE 1. Computational domain for the plane diffuser. Only a subset of the actual grid lines is plotted. All streamwise distances are measured as distance from the entrance of the expanding section in units of δ .

2. Accomplishments

2.1 Numerical method

The numerical method for solving the unsteady, incompressible Navier-Stokes equations is described in Choi *et al.* (1993). Second-order spatial central differences on a staggered mesh are combined with a fully-implicit time integration scheme (Crank-Nicholson) which uses Newton linearization along with approximate factorization. Approximately 4 iterations per time step are required to reduce the residual sufficiently when running the code at CFL ranging from 2 to 3. The cost is therefore comparable to an explicit scheme running at CFL smaller than 1. In this type of flow the CFL-limit is set through the wall-normal velocity in the vicinity of the rounded entrance corner. For a typical grid of $163 \times 64 \times 64$ cells the code runs at 350 Mflops and requires 20 μ s per cell per time step on a Cray C-90.

Unsteady data, created in an independent LES of fully developed channel flow, are specified at the inflow plane. A convective boundary condition, i.e. $\partial u_i / \partial t + c \partial u / \partial x = 0$, is applied at the outflow plane, where c is the bulk velocity of the outlet channel. The upper and lower boundaries are no-slip walls.

A simple, robust version of the dynamic SGS model (Germano *et al.* 1991) in combination with least-square contraction (Lilly 1992) and spanwise averaging is used. The total viscosity is constrained to be positive through a clipping operation.

2.2 Grid spacing requirements

The dimensions of the computational domain are shown in Fig. 1. The diffuser geometry and the Reynolds number $Re_b = U_b \delta / \nu = 9000$ match the experimental configuration of Obi *et al.* (1993). Here, U_b denotes the bulk velocity of the incoming fully developed turbulent channel flow of height 2δ . The flow from the inlet channel of length 5δ enters an asymmetric diffuser with an expansion ratio of $a = 4.7$ and an opening angle of approximately 10° . The expanding section extends over 42δ . The outlet section is too short to cover the full recovery, but no measurements were reported beyond $x = 58\delta$. Both corners are rounded with a radius of 8.6δ . Due to the high resolution requirements in the spanwise direction, the computational domain could not be chosen larger than 4δ , resulting in aspect ratios of inlet and outlet channel of 1 : 2 and 1 : 0.43, respectively. The experiment had much higher aspect ratios of 1 : 35 and 1 : 7.45, respectively.

Previous studies have shown that proper simulation of the near-wall region without employing a near-wall model imposes severe limits on the spanwise grid-spacing.

With the present numerical method, a spanwise spacing of $\Delta z^+ = 15$ can be tolerated for a canonical boundary layer or a developed channel flow at this Reynolds number before results deteriorate significantly. Resolution requirements are highest in the inlet channel where the flow is attached. At $Re_b = 9000$ we expect Re_τ close to 500 and a wall-unit approximately 0.002δ . We therefore used 128 points in the span for a width of 4δ , corresponding to $\Delta z^+ = 15.5$, for the *inflow data creation run*, but not for the actual diffuser LES.

Span-wise resolution requirements decrease further downstream because of the increase of a wall-unit due to the channel expansion. Additionally, near-wall physics change under an adverse pressure gradient and resolution requirements become less severe. Therefore, the following approach can be justified: the inflow data are created on a fine mesh; at the inflow plane we use unsteady data which are filtered onto a mesh which has only half of the spanwise resolution of the inflow creation run ($\Delta z^+ = 30$). We find that this method works quite well and does not give significantly different results from a case where the fine spanwise resolution was carried through the whole diffuser. A similar approach was used by Akselvoll (1994) for simulation of flow over a backward-facing step.

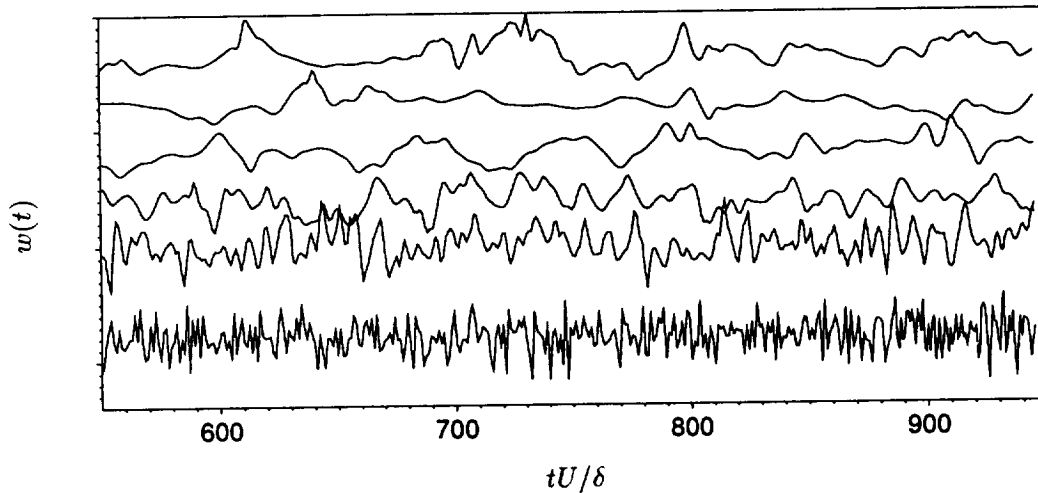


FIGURE 2. Time series of spanwise velocity fluctuations from LES at stations $x = 11, 20, 26, 35, 45,$ and 61 , from bottom to top, recorded close to the diffuser centerline.

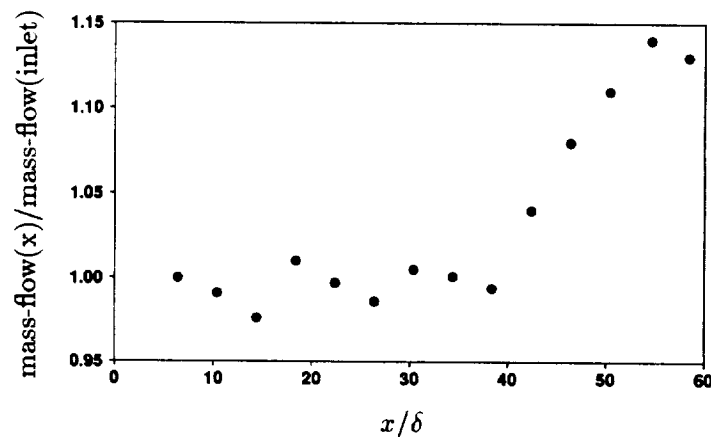
2.3 Simulation time requirements

As was the case with the *spatial* resolution, we find that the flow inside the diffuser imposes very different requirements with respect to the *temporal* resolution in the inlet and outlet sections. The inertial time scale $\tau = 0.5h(x)/U_b(x)$, based on local diffuser height $h(x)$ and bulk velocity $U_b(x)$, increases with the square of the expansion ratio from the inlet to the outlet section, i.e. $\tau_{out} = a^2\tau_{in}$. In order to properly simulate the inlet turbulence and due to CFL-limits, the maximum

time-step is approximately $0.1\tau_{in}$. Statistics in the outlet section will converge after a minimum of $50\tau_{out}$ or 12000 time-steps. The total cost of one simulation is 100 CPU hours, of which 40% were spent reaching a statistical steady state. The order-of-magnitude time scale change which occurs as the flow slows down inside the expanding section becomes evident in the time series of spanwise velocity fluctuations measured at several streamwise locations (Fig. 2).

2.4 Assessment of the experiment for validation purposes

The experiment by Obiet *al.* (1993) was done in an open loop wind tunnel facility. The flow entered the diffuser after a rather long development section of 200δ . The wide aspect ratios of 1 : 35 and 1 : 7.45 for inlet and outlet duct guaranteed a spanwise homogeneous core flow over 90% of the inlet and 60% of the outlet span. An increase of mass-flow along the core section of the diffuser was found in the experiment, see Fig. 3. The rather strong increase (more than 10%) downstream of $x = 40$ indicates that a secondary flow develops in the outlet section. It is unclear whether the flow upstream of $x = 40\delta$ is affected by this phenomenon. If not, it can be used for validation purposes of a simulation which assumes spanwise homogeneity of turbulence to avoid explicitly accounting for side walls.



dvips FIGURE 3. Mass-flow ratio as obtained from integrating measured velocity profiles over the local diffuser height.

Measurements have been rescaled individually for each streamwise location in order to make them consistent with a constant mass-flow through the inlet duct. It is probably safe to use data upstream of $x = 40$ for validation purposes. Flow separation occurs a substantial distance (20δ) upstream of the location with the mass-flow problem. It seems unlikely that the flow at this location is affected by the secondary flow in the outlet section. Additional support for this hypothesis comes from the fact that flow statistics did not change when we performed a simulation on a domain where the outflow boundary was inside the expanding section.

The secondary flow causes additional pressure losses, which would not be present in a spanwise homogeneous case. This becomes evident when a force balance for

a control volume formed by a vertical x, y cross-section and with unit depth is computed from the experimental data.

2.4.1 Force balance

An integral force balance indicates whether a simulation has reached statistical equilibrium and gives insight about the relative importance of frictional losses. Additionally, a force balance is a good check of the suitability of the pressure measurements for validation purposes.

The control volume for the force balance in the streamwise direction is formed by a plane through the inlet duct at x_{in} , a plane perpendicular to the flat wall somewhere inside the diffuser at x_{out} , and through cuts along upper and lower diffuser walls. The balance for a volume with unit depth and under the assumption of constant pressure across the diffuser reads

$$\sum F_x = -F_{pressure} - F_{friction} - F_{ramp} = \dot{J}|_{x_{out}} - \dot{J}|_{x_{in}}$$

with the (positive) forces defined as

$$F_{pressure} = (p_{x_{out}} - p_{x_{in}})h_{x_{in}}, \quad F_{friction} = \int_{x_{in}}^{x_{out}} \tau_w(l) \cos \alpha(l) dl,$$

$$F_{ramp} = \int_{x_{in}}^{x_{out}} (p_{x_{out}} - p(l)) \sin \alpha(l) dl, \quad \dot{J} = \rho \int_0^{h(x)} U(y)^2 \text{sign}(U) dy .$$

The angle formed by the wall and the horizontal is denoted α . Fig. 4 depicts the various contributions to the force balance as a function of location x_{out} . The inlet station was fixed at $x_{in} = -3$. For the experiment, no data were available for the inlet velocity profile and skin friction. We assumed a $y^{1/7}$ power law for the mean velocity at the inlet, which gives about the right ratio U_{cent}/U_b . For the skin friction we used data from the simulation. As will be shown later the frictional losses play a minor role in the force balance.

The terms of the right-hand side of the force balance are normalized with the left-hand side (l.h.s), i.e. the momentum flux difference across the control volume. Once steady state has been reached, the normalized l.h.s. should sum up to 100%, which is approximately the case for the simulation data, independently from where the control volume is located. A small residual of 2% stems from approximations involved in the evaluation of the individual forces. The difference in momentum flux is mainly balanced by the pressure gain throughout the diffuser. Roughly 30% of the momentum loss is converted into a force acting on the inclined wall. Friction from the top and bottom walls accounts for less than 5% of the momentum losses. Even a 20% change in the skin friction changes the overall balance by only 1%.

If we compute the force balance from the experimental data, we find a rather large residual in the range from 20% to 30% of the momentum flux difference. Possible

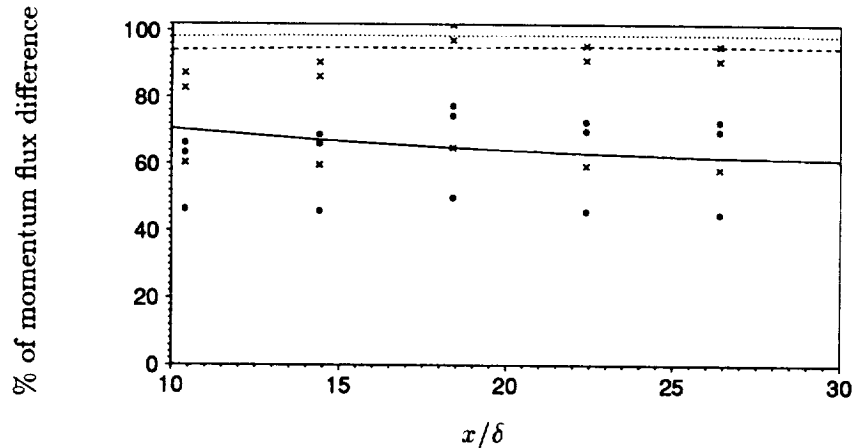


FIGURE 4. Force balance for plane diffuser: accumulated forces F_{press} (—), $F_{press} + F_{ramp}$ (---), and $F_{press} + F_{ramp} + F_{frict}$ (·····), from LES, normalized by the momentum flux difference as a function of the location of the downstream control volume face. The upstream face is fixed at $x = -3$. Balance computed from original data of Obiet *al.* (1993) (•) and with c_p enhanced by a factor of 1.3 (×).

reasons include measurement errors (wrong reference velocity or density for c_p), deviations from spanwise homogeneity, and additional pressure losses resulting from secondary flow in the diffuser outlet. The additional frictional losses which stem from the diffuser side walls can be neglected because the side wall surface area is rather small compared to the upper and lower walls of the experimental facility. The most likely source for the momentum deficit is the use of a wrong reference velocity for computation of c_p . In the original data set, mean velocities were scaled in such a way that the corresponding ratio of centerline to bulk velocity in the inlet section would be 1.05, which is quite different from the independently measured value for this ratio of 1.14. The source for this mismatch is obviously the use of devices (Pitot tube, hot-wire, LDA) which were not properly calibrated or aligned.

Possibly, the same problem appears with normalization of pressure measurements. However, as discussed earlier, the pressure rise inside the diffuser will be strongly affected by the presence of a secondary flow. Blockage from side wall boundary layers increases the velocity in the center of the duct and limits the pressure recovery. If the momentum deficit was purely caused by usage of a wrong reference velocity, a 'valid' c_p curve can be reconstructed by rescaling the measured c_p . The rescaling factor can be determined by requiring that the residual for the force balance vanish. Fig. 4 includes the force balance for the experimental data set, which was obtained when c_p was increased by 30%. This corresponds to a 14% decrease in reference velocity. With this correction, the residual drops below 5%.

Despite the problem with the pressure measurements, we think that the experiment is valuable and can be used for validation purposes, at least upstream of $x = 40$. From the close coupling between mean flow profile shape and c_p -curve,

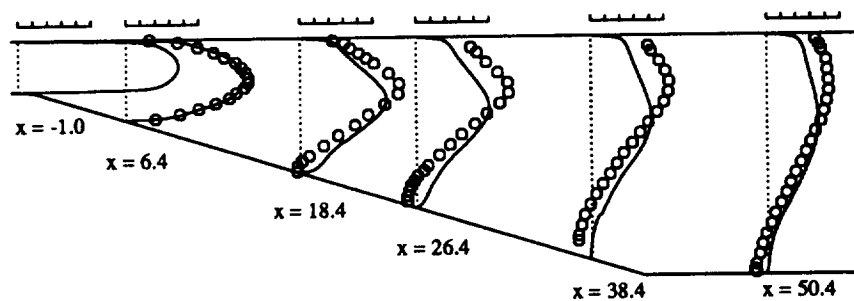


FIGURE 5. Mean velocity $U/U_{b,in}$ from LES (—) and experiment (o). Increments of the scales are 0.1.

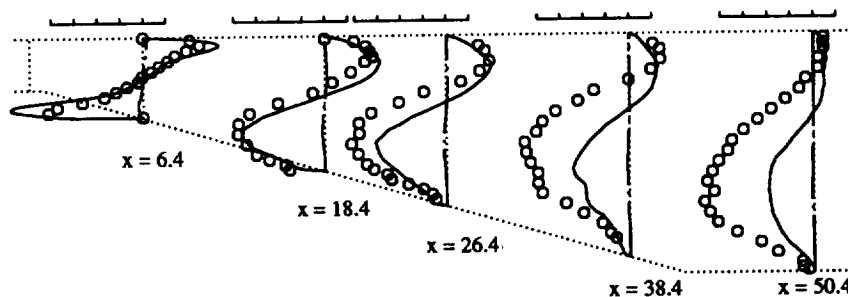


FIGURE 6. Turbulent shear stress $\overline{uv}/U_{b,in}^2$ from LES (—) and experiment (o) and SGS-stress τ_{12} (---). Increments of the scales are 0.001.

it follows that it is sufficient to either match the mean flow or the c_p -curve as an indicator for proper prediction of the flow if only one of these quantities is available.

2.5 Simulation results

Flow statistics were obtained by averaging simulation results in time and in the spanwise homogeneous direction. We compare results from a LES with measurements of Obi *et al.* (1993).

All data are scaled with the bulk velocity from the inlet channel, $U_{b,in}$. The ratio of centerline to bulk velocity in the inlet channel was 1.10 in the simulation and 1.14 ± 0.02 in the experiment. Profiles of mean velocity are strongly asymmetric inside of the expanding section, see Fig. 5. The flow remains attached on the flat wall and separates about halfway down the ramp. The LES exhibits only minimal backflow between $x = 30$ and $x = 50$ whereas measurements show significant backflow downstream of $x = 18$. Profiles of components of the Reynolds stress tensor are shown in Figs. 6, 7 and 8. We depict only the resolved motion part of the normal stresses \overline{uu} and \overline{vv} from the LES because the SGS kinetic energy is not explicitly known in our SGS-model. Fig. 6 shows that the off-diagonal components of the SGS-stresses are negligible when compared with the resolved scale turbulent shear stress \overline{uv} .

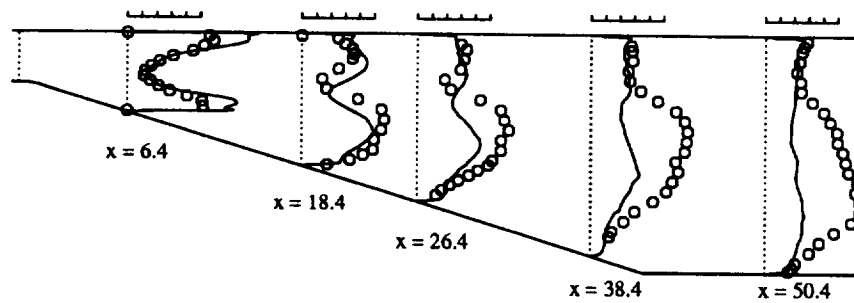


FIGURE 7. Streamwise velocity variance $\overline{uu}/U_{b,in}^2$ from LES (—) and experiment (\circ). Increments of the scales are 0.002.

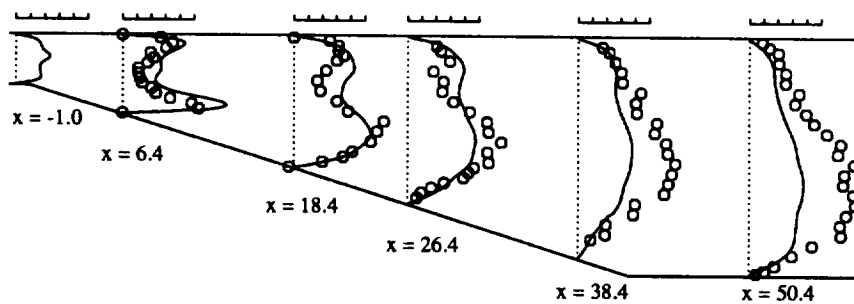


FIGURE 8. Vertical velocity variance $\overline{vv}/U_{b,in}^2$ from LES (—) and experiment (\circ). Increments of the scales are 0.001.

Simulated and measured Reynolds stresses agree within some scatter up to location $x = 14.4$ (not shown). Further downstream, the simulation exhibits a much lower core flow turbulence level than the experiment. Mean flow profiles begin to deviate at station $x = 10$. The satisfactory match of simulation and experiment in the entrance part of the diffuser indicates that the inlet condition for the simulation, i.e. fully developed channel flow, was adequate. Additionally, we found that this flow is not very sensitive to the quality of the inflow database. Underprediction of separation leads to a quicker pressure recovery in the simulation compared with the (rescaled) experimental data, see Fig. 9.

2.6 Discussion

The outcome of this simulation does not give a clear picture about the success or failure of LES to predict the flow inside the diffuser. The following discussion is based on more simulation data than presented in this report. We have performed a series of simulations on finer meshes where we varied the spacing in all three directions, for example Δz^+ between 12 and 40. A good measure for the role of the SGS model in this type of simulation is the contribution of the SGS stresses to the total energy dissipation rate, which varied from less than 50% on fine meshes to more than 80% on coarse meshes (see Fig. 10).

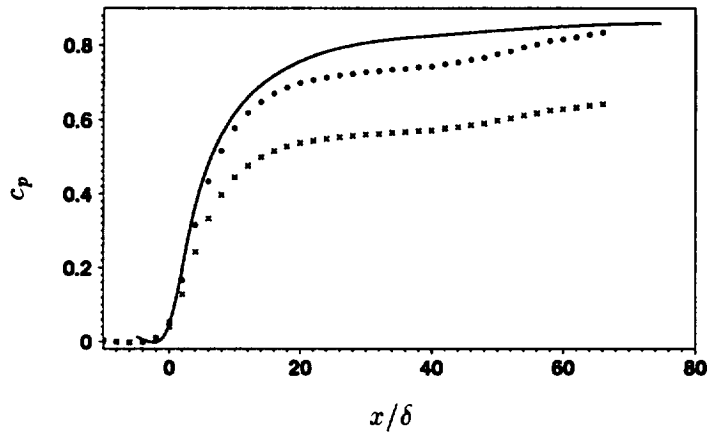


FIGURE 9. Pressure coefficient c_p , based on $U_{b,in}$, along lower diffuser wall. Results from LES (—), original experimental data (\times) and data scaled with 1.3 (\bullet).

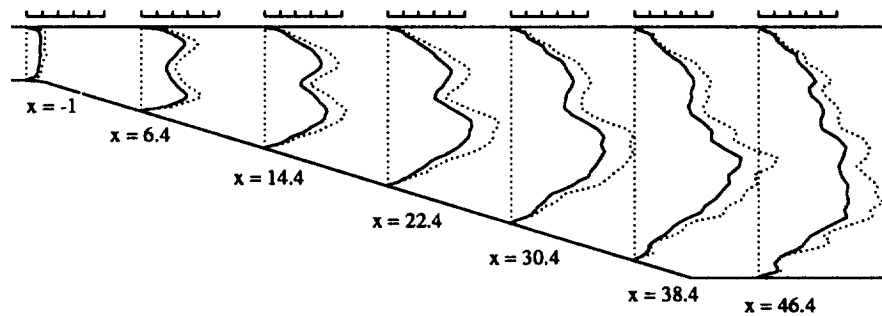


FIGURE 10. Ratio of SGS-eddy viscosity and molecular viscosity (—) and of corresponding dissipation rates (----) from LES. Scale increments are 1.

The LES solutions obtained on various meshes differ with respect to pressure recovery by less than 4% and overpredict c_p by roughly 10% when compared with the *rescaled* experimental data, see Fig. 9. This proves the capability of the dynamic procedure to adapt the role of the SGS model to a given grid resolution. Our simulations are in this sense ‘grid-independent’. We also found that the flow changes quite drastically (on the coarser meshes) when the SGS model is turned off, indicating the importance of an adequate SGS model for this type of simulation.

We also checked the sensitivity of results with respect to the spanwise domain size, which we varied between 4δ and 12δ . Again, the flow inside the diffuser turned out to be rather insensitive with respect to this parameter.

There is also the possibility of a non-adequate numerical scheme which might have an even stronger impact on the simulation than specific properties of the SGS model. Although the discretization of the non-linear term is strictly energy conserving on a

Cartesian mesh, this property might be violated on stretched meshes. This aspect is the topic of an ongoing evaluation of the numerical scheme.

3. Conclusions and future plans

We find that LES of flow through the plane diffuser gives a consistent, grid-independent result. The dynamic model seems to work fine in an adverse pressure gradient situation although the present simulation underpredicts separation when compared with measurements. The cost of the simulation is set by the high spatial resolution requirements of the inlet section and the rather long simulation time caused by the presence of a very wide range of time scales. Use of zonal techniques or unstructured meshes (see article by Ken Jansen in this volume) would be desirable and could strongly reduce the overall cost.

The cause for deviation between LES results and measurements has not been fully understood yet. The experimental data have some obvious flaws in terms of momentum balance and mass conservation. However, we are not so much concerned about the lack of reliable pressure measurements for validation purposes. For the present flow, the shape of the mean flow profiles is a very sensitive indicator for the quality of flow prediction and partially compensates for the lack of c_p .

A fully-resolved DNS for this case would be very costly (in the order of 1000 CPU hours) but could be done on present computers. This would eliminate all doubts about the 'right' flow to compare with. We will further investigate this case by improving the numerics, using schemes with higher-order truncation errors. As a further goal, we plan to investigate whether a LES with a near-wall model is able to describe this flow adequately at a much lower cost than the present simulation.

REFERENCES

- AKSELVOLL, K. 1994 Personal communication.
- CHOI, H., MOIN, P. & KIM, J. 1993 Direct numerical simulation of turbulent flow over riblets. *J. Fluid Mech.* **255**, 503-539.
- DURBIN, P. 1994 Separated flow computations with the $k - \epsilon - v^2$ model. *CTR Manuscript 152*. NASA Ames/Stanford Univ.
- GERMANO, M., PIOMELLI, U., MOIN, P. & CABOT, W. H. 1991 A dynamic subgrid-scale eddy viscosity model. *Phys. Fluids A*. **3**, 1760-1765.
- LILLY, D. K. 1992 A proposed modification of the Germano subgrid scale closure method. *Phys. Fluids A*. **3**, 2746-2757.
- OBI, S., AOKI, K. & MASUDA, S. 1993 Experimental and computational study of turbulent separating flow in an asymmetric plane diffuser; in: *Ninth Symposium on Turbulent Shear Flows*, Kyoto, Japan, August 16-19, 1993. p. 305.
- SIMPSON, R. L. 1989 Turbulent boundary-layer separation. *Ann. Rev. Fluid Mech.* **21**, 205-234.